Impact of Solar Salt aging on corrosion of martensitic and austenitic steel for concentrating solar power plants

Alexander Bonk[a,1,*], Dagmar Rückle[b,1], Stefanie Kaesche[b], Markus Braun[a], Thomas Bauer[c]

[a]*German Aerospace Center (DLR), Institute of Engineering Thermodynamics, 70569 Stuttgart, Germany*
[b]*Materialprüfungsanstalt University of Stuttgart, Referat Korrosion, 70569 Stuttgart, Germany*
[c]*German Aerospace Center (DLR), Institute of Engineering Thermodynamics, 51147 Köln, Germany*

Abstract

This work addresses the influence of molten nitrate salt chemistry on the corrosion behavior of a martensitic high temperature steel and an austenitic stainless steel. It is one of the first addressing controlled degradation of Solar Salt by controlling the gas atmosphere on top of the melt, thus driving the formation of corrosive ions, mainly oxide ions but also nitrite ions. The stainless steel and high temperature steel samples are subjected to the different operating conditions to demonstrate the variations in corrosivity as a function of gas atmosphere and additionally of artificially added chloride impurities. The results indicate that the atmosphere has a direct impact on the formation of corrosive oxide and nitrite ions. The low Cr-steel is found to be more sensitive to chloride impurities, while the stainless steel corrosion is enhanced by the presence of nitrites and oxide ions. All studies are supported by profound molten salt analysis throughout the experiments including the analysis of nitrate, nitrite, oxide and chromate ions as well as cation compositions. Steel samples are analyzed by scanning electron microscopy methods and corrosion rates are extrapolated from 1200 h experiments.

Keywords: Molten Salt Corrosion, Nitrate Salt, Thermal Energy Storage, Concentrating Solar Power, Thermal Stability

*Corresponding author
Email addresses: alexander.bonk@dlr.de (Alexander Bonk), dagmar.rueckle@mpa.uni-stuttgart.de (Dagmar Rückle)

[1]Both authors contributed equally to this work.

1. Introduction

Molten nitrate salts are state-of-the-art storage media in modern concentrating solar power plants coupled with a thermal energy storage (TES) unit.[1, 2] Operating temperatures are in the range of 290 °C up to 565 °C for classical Solar Salt, a non-eutectic mixture of $NaNO_3$-KNO_3 (60–40 wt %).[3–5] During a charging cycle molten salt from a cold tank (at 290 °C) is pumped through e.g. the solar tower and heated to 565 °C after which it is pumped into a hot tank (operated constantly at 565 °C) either for storage or steam generation with a steam turbine.[1, 6] Although Solar Salt is considered particularly stable, its chemistry can be affected by the operating temperature over time.[7] It is well established that molten nitrate salts form nitrites as a function of temperature and oxygen partial pressure according to Nissen and Meeker [8]:

$$NO_3^- \rightleftharpoons NO_2^- + \frac{1}{2}O_2 \tag{1}$$

Under typical operating conditions, e.g. 560 °C and a constant oxygen partial pressure of 0.2 atm, a nitrite content of 4.5 mol % (or 2.5 wt % with regard to the total salt mass) establishes as shown by other studies and in our own work recently.[7–10] Further decomposition reactions can be observed at high temperatures which, in the first place, involve further decomposition of the nitrite ion into oxide ions (e.g. O^{2-}) and different gaseous species such as nitrous gases (NO, NO_2), nitrogen (N_2) or oxygen (O_2). Some of the proposed reactions are shown in equation 2 and 3.[11, 12]

$$2NO_2^- \rightleftharpoons O^{2-} + NO + NO_2 \tag{2}$$

$$5NO_2^- \rightleftharpoons O^{2-} + N_2 + 3NO_3^- \tag{3}$$

The decomposition reactions are critical due to the formation of toxic nitrous gases [13] and even more so oxide ions that are supposed to aggravate corrosion.[14, 15] According to Desimoni et al. [16, 17] the hyperoxide ion (O_2^-) can easily be oxidized to a peroxide ion (O_2^{2-}) or even a superoxide ion (O_2^-) via a nitrate-nitrite redox reaction, but their presence and stability depends on the cation fractions in the molten salt. Despite, all species play an important role in the corrosion of steel, as summarized by

e.g. Fernández et al. [18]. The oxides formed by equation 2 can lead to the oxidation of iron according to the redox reaction shown in equation 4:

$$6(\mathrm{KNa})\mathrm{NO_3} + 4\mathrm{Fe} \rightleftharpoons 2\mathrm{Fe_2O_3} + 6(\mathrm{KNa})\mathrm{NO_2} \tag{4}$$

It is commonly accepted that different layers of oxides form during the corrosion process of stainless steels and high temperature steels in molten salts.[19] When iron oxidizes at high temperatures in air or molten salts, different oxides can form on the surface. More precisely, iron is oxidized while the nitrate ions of the molten salt are reduced to form nitrite (Eq. 4). Further iron oxidation depends on the stability of the primary formed oxides. Below 570 °C two iron oxides namely Fe_3O_4 (magnetite) or Fe_2O_3 (hematite) can form.[19] Above 570 °C a third Fe-rich phase namely FeO (wustite) becomes a stable species.[20] According to Pinder et al. [21] primarily magnetite is formed on the whole surface until complete coverage and then the oxide layer thickness grows parabolically. Subsequently, the nucleation of hematite starts on top of the magnetite layer and its growth rate decelerates. By the addition of different alloying elements like chromium, aluminum, silicon or molybdenum the high temperature behavior of materials can be influenced significantly.

In this work, the impact of molten salt chemistry, changed by the gas atmosphere, and artificial chloride impurities on the corrosion behavior of SS 316Ti and AISI A213/T91 is investigated.

2. Materials and Methods

Solar Salt has been mixed from $NaNO_3$ (>99.5 %, Merck, Germany) and KNO_3 (>99.5 %, Merck, Germany) precursors with *pro analysis* grade. For specific experiments (see) 0.5 wt % chloride impurities were added using a NaCl (>99.9 %, Merck, Germany) precursor. Trace analysis of the precursor salts by ion chromatography and acid base titration (see upcoming paragraphs) revealed no presence of impurities critical for the corrosion process such as magnesium ions, hydroxides, sulfates or phosphates.

For isothermal treatment two setups were used - an autoclave test rig for experiments without chloride impurities, and a modified convection furnace for experiments with molten salts containing chloride impurities. The main reason for two setups are constraints regarding the number of available autoclave test rigs.

The autoclave test rig and experimental conditions employed have already been described elsewhere in detail.[22] To present a short summary a section of this recent study is quoted hereafter. " *The sample chamber consists of tubular stainless steel with an inner diameter of* 56.3 mm *and an inner height of* 190 mm*. The tube was welded on a flange, which was sealed with a top flange. A total of five holes in the top flange were used for stirring (*$1\,\mathrm{U\,min^{-1}}$*), thermocouples (type* K*), pressure control (pressure valves, analogous manometer) and gas inlet and outlet. The latter is connected to a separator to keep aerosols from exiting the chamber. The last hole was used to extract samples from the melt. Experiments were conducted in a continuous flow of gases (*$100\,\mathrm{mL\,min^{-1}}$*) on top of the melt. The molten nitrates are filled into an alumina crucible which is placed in the tubular stainless steel chamber. The steel chamber itself is placed in a heated and insulated block. Heating is performed over a height of* 60 mm *on the chamber walls.* "[22]

In the modified convection furnace the same types of crucibles are used and nine crucibles are used simultaneously in the oven chamber. Flanges seal individual crucibles (see images in ref. [22]), which protrude from the furnace to avoid salt creeping to the flange. The molten salt is not stirred during the experiments performed in the convection furnace.

In all cases the alumina crucibles were purged with either high purity N_2 gas (purity 5.0) or synthetic air (s.a.) (20 vol % O_2, 80 vol % N_2, both 5.0 grade). Molten salt samples were extracted throughout all experiments in the autoclave test rig, but only after the whole experiment in the convection furnace. The molten salt chemistry was investigated using cation and anion chromatography as well as acid-base titration to detect nitrate, nitrite, oxide, carbonate and chromate ions in the molten salt samples. A statistical analysis of the chromatography tool as well as more detailed sample preparation techniques have been provided in one of our last publications in more detail.[22]

Two steel types were used for corrosion experiments: AISI 316Ti and AISI A213

Table 1: List of experiments including salt type, atmosphere on top of the melt, steel type and the number of salt samples extracted throughout the individual experiments. All experiments were performed at 560 °C for 1200 h. The *Exp.-ID* comprises the steel type, atmosphere (SA: synthetic air, N2:N_2) on top of the melt, presence or absence of chloride impurities (*Cl*), with repeated experiments featuring an *r*.

Exp.-ID	**Salt**	**Atmosphere**	**Steel type**	**N° salt samples extracted**
blankSA	Solar Salt	Air	-	9
blankN2		N_2	-	11
316SA	Solar Salt	Air	AISI 316Ti	7
316SAr			AISI 316Ti	7
213SA			AISI A213	7
213SAr			AISI A213	7
316N2	Solar Salt	N_2	AISI 316Ti	7
316N2r			AISI 316Ti	7
213N2			AISI A213	8
213N2r			AISI A213	7
blankN2Cl	Solar Salt	Air	-	2
blankSACl		N_2	-	2
316SACl	Solar Salt +0.5 wt%Cl^-	Air	AISI 316Ti	2
316SAClr			AISI 316Ti	2
213SACl			AISI A213	2
213SAClr			AISI A213	2
316N2Cl†	Solar Salt +0.5 wt%Cl^-	N_2	AISI 316Ti	2
316N2Clr			AISI 316Ti	2
213N2Cl†			AISI A213	2
213N2Clr			AISI A213	2

†: gas flow was blocked during experiments

/ T91 steel. All steel samples were ground prior to the experiments using SiC grinding paper until 600 grit size. The sample size and weight were measured and finally samples were cleaned and dried. Each steel type was stored in 100 g of Solar Salt at 560 °C for around 1200 h and removed after the experiment. Samples were cleaned with deionized water, dried under hot air, weighed and scanning electron microscopy (SEM) analysis was performed (Zeiss ESEM EVO LS15 with LaB_6-cathode) to gain the structure of the formed oxide layers on the sample surfaces. Afterwards the oxide layers were removed by etching and samples were finally weighed and SEM analysis of the blank surfaces was performed to gather information about the corrosion attack.

The corrosion rate (CR) in $mm\,a^{-1}$ was determined according to DIN 50905-1 using Eq. 5.[23]

$$CR = 8.76 \cdot \frac{\Delta m}{A \cdot t \cdot \rho} \tag{5}$$

where Δm is the mass loss of the sample after pickling, A is the surface area of the sample, t is the time of exposure, and ρ is the density of the bulk metal.

Samples of 316Ti and A231/T91 were exposed to chloride free solar salt at 560 °C for 1008 h. Afterwards sample cross sections (FIB cuts) were done by use of a cross-beam workstation (Zeiss Auriga) and the during the corrosion process at the interface between steel and melt formed oxide layers were characterized by means of energy dispersive X-ray spectroscopy (EDX). Layer structure, thickness, chemical composition and adhesion to the steel surface with special regard to the ability to protect the steel from further corrosive attack were studied.

3. Results & Discussion

Molten Salt Chemistry during corrosion experiments

The molar content of nitrates and nitrites in Solar Salt in which the steel samples were immersed at 560 °C under synthetic air (s.a.) atmosphere, is shown in Figure 1. It has to be emphasized, that successive sample extraction was only carried out in the autoclave test rig. For all experiments in this setup nitrite ions form during the first few hours of the experiment, while the nitrate content decreases accordingly. Both indicates

the equilibration of the nitrate-nitrite chemistry under constant oxygen partial pressure of the synthetic gas atmosphere as presented earlier in equation 1. The nitrite content, when in equilibrium, is in the range of 4.7 mol% to 5.3 mol% while the remaining nitrate content is 94.3 mol% to 95.7 mol%. Most importantly, the same molten salt chemistry is observed during the first- and the repeated experiments indicating high reproducibility. During the experiments in the convection furnace the final nitrite and nitrate levels were very similar, namely between 4.3 mol% to 6.3 mol% and 93.4 mol% to 94.6 mol%, respectively at the end of the experiment. It is reasonable to assume that the molten salt chemistry is in equilibrium for all experiments under s.a.. More importantly, results demonstrate that the experimental conditions are comparable in both setups, the autoclave test rig and the modified convection furnace and therefore the corrosion results can be considered comparable.

The molten salt chemistry changes drastically when Solar Salt is stored under N_2-atmosphere. Successive sample extraction in the autoclave test rig shows steadily decreasing nitrate contents over time for all experiments, as shown in Figure 2. For the blank salt experiment (*AblankN2*), the nitrate content decreases to a level of 63.73 mol %, while the nitrite level increases steadily up to 35.97 mol % after 1000 h. This in turn shows that no equilibrium nitrate-nitrite level is formed due to the constant removal of gaseous oxygen formed by reaction 1. During the oxidation of AISI 316Ti in Solar Salt (*316N2*) the nitrate decomposition (and nitrite formation) is even more pronounced compared to the blank experiment indicating a slightly higher rate of molten salt degradation. The nitrite formation rate at first remains linear up to 800h, while it slightly decreases towards the end of the experiment with final nitrate / nitrite levels of 49.8 mol % / 49.9 mol % in the original (*316N2*), and 49.7 mol % / 50.14 mol % in the repeated (*316N2r*) experiment.

For the AISI A213/T91 significantly less molten salt degradation is observed. The nitrate levels during the original experiment (*213N2*) only decreased to 71.8 mol % with nitrite levels of 27.9 mol %. In the repeated experiment (*213N2r*) values are much higher (as originally expected), in the range of 57.8 mol % NO_3^- / 42.2 mol % NO_2^-. The differences in decomposition rates were identified to be a result of technical constraints which involved molten salt evaporation into the gas inlet/outlet which blocked

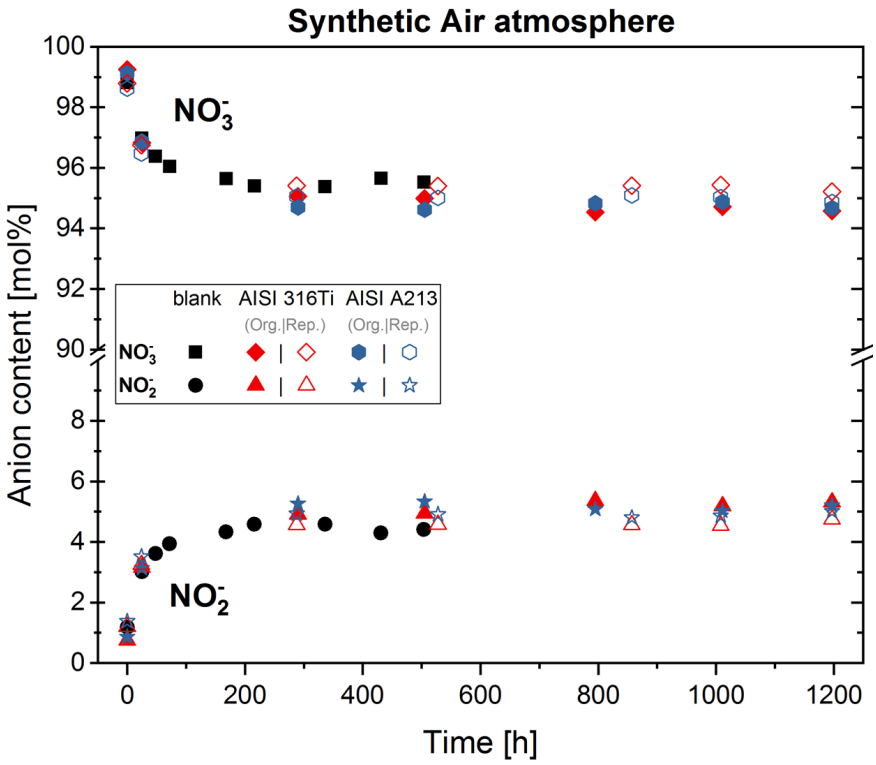

Figure 1: Nitrate and nitrite content in Solar Salt stored with AISI A213/T91 and AISI 316Ti under s.a. atmosphere in the autoclave test rig (without chloride impurities). Values gained from original experiments are shown using filled symbols while repeated experiments are represented by open symbols.

the gas flow. Thereby the gas products formed during Solar Salt decomposition were not effectively removed from the crucible but remained close to the melt, thus shifting equilibrium to the nitrate side.

Studying the oxide levels in the molten salts (Figure 3), the expected decomposition reaction (Eq. 2/3) can be observed. While under s.a. no significant level of oxide ions is detectable, steadily increasing oxide ion concentrations are detected for all sets of experiments performed under N_2-atmosphere.

The formation of oxides can be ascribed to decomposition reaction 2 or 3 but it has to be emphasized that the *actual* type of oxides ions cannot be distinguished by the analytic methods applied. Consequently, oxide ions are always regarded as O^{2-}

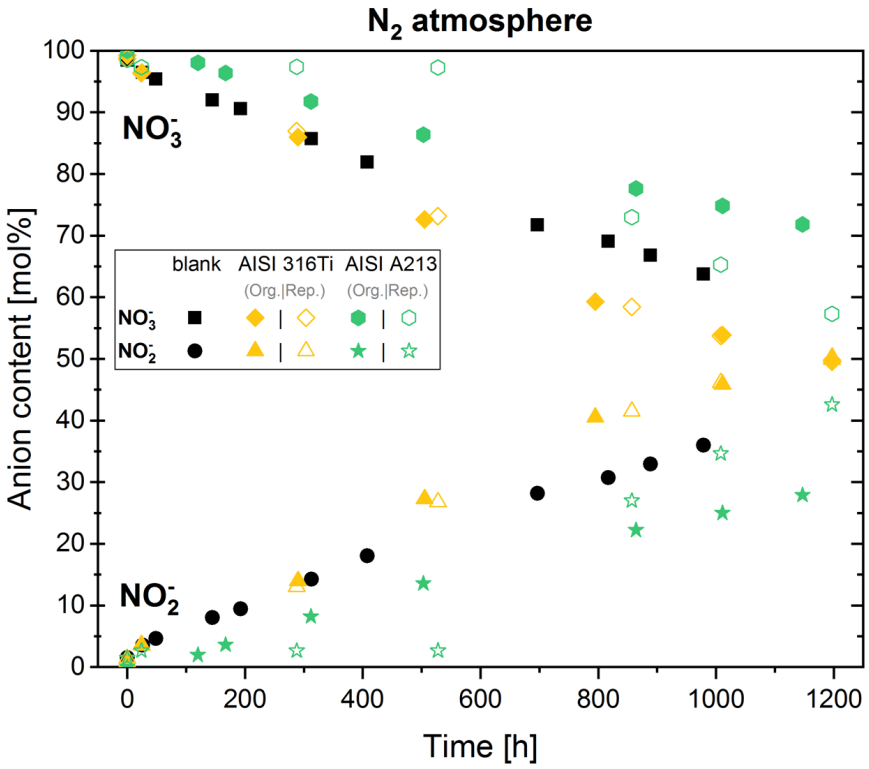

Figure 2: Nitrate and nitrite content in Solar Salt stored with AISI A213/T91 and AISI 316Ti under nitrogen atmosphere in the autoclave test rig (without chloride impurities).

for clarity. The acid-base titration used for the analysis of oxide levels, can also be used for the detection of other basic ions such as carbonates.[9] Their content is also shown in Figure 3 but it is not obvious why carbonates form under a synthetic gas / N_2-atmosphere after all. Traces of CO_2 may have leaked into the test rig during sample extraction or may :

$$CO_2 + O^{2-} \longleftrightarrow CO_3^{2-} \tag{6}$$

Carbonates are not expected to influence corrosion, but rather contribute to corrosion-erosion phenomena due to the formation of partly insoluble metal carbonate species.[24] In our studies we observed successively higher carbonate contents in experiments performed under s.a. than under N_2 which may indicate higher levels of CO_2 in the s.a.

supply. Overall, the carbonate levels are however too low to form insoluble carbonate species at the elevated temperatures.[25] Therefore, it can be assumed that erosion phenomena did not contribute to the overall corrosion process.

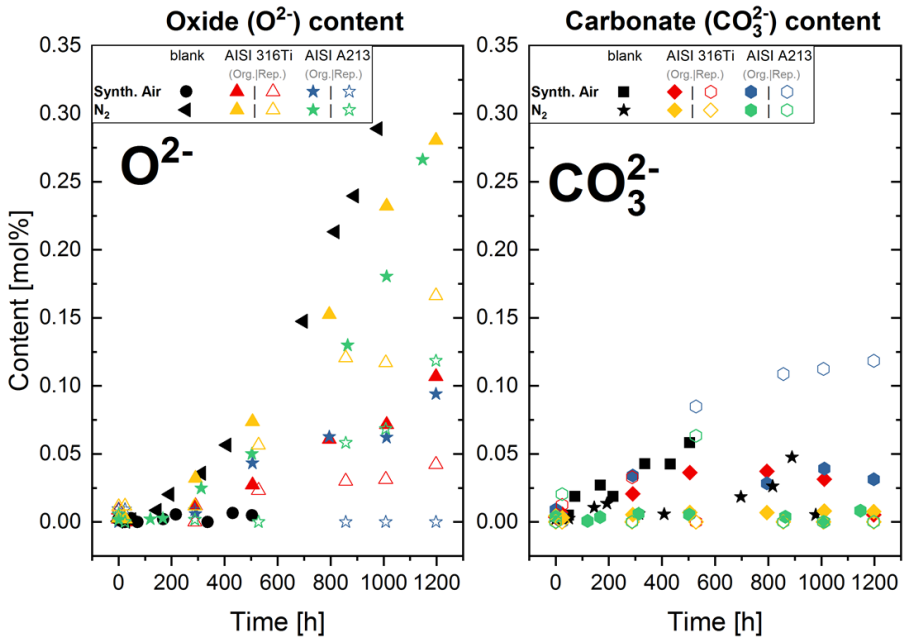

Figure 3: Molar contents of oxides (left) and carbonates (right) in Solar Salt stored with AISI A213/T91 and AISI 316Ti under s.a. and N_2 in the autoclave test rig.

For the experiments performed in the convection furnace, only two samples were extracted at the start and at the end of the experiment. The composition of the molten salt samples at the end of the experiment in terms of nitrate, nitrite, oxide and carbonates is shown in Table 2 for both, original and repeated experiments. The molten salt chemistry under s.a. behaved similar to that observed in the autoclave test rig where the nitrate and nitrite levels are in the range of 93.4 mol% to 95.5 mol% and 4.31 mol% to 6.28 mol%, respectively, and mainly carbonates are observed as impurities for the original and the repeated experiments.

Under N_2-atmosphere during the original experiments however, only the blank experiment (*blankN2Cl*) behaved as expected, with a very high decomposition rate of

Table 2: Molten salt chemistry at the end of the storage experiments (1200 h) in the convection furnace (including 0.5 wt%Cl^- impurities). Values from the repeated experiments are shown in brackets.

Steel type	Gas	Anion content [mol%]			
		NO_3^-	NO_2^-	O^{2-}	CO_3^{2-}
blank		94.93 (93.83)	4.92 (5.66)	0.06 (0.06)	0.08 (0.45)
AISI 316Ti	Synth. Air	94.56 (93.43)	5.24 (6.28)	0.13 (0.00)	0.07 (0.29)
AISI A213/T91		95.50 (95.11)	4.31 (4.74)	0.00 (0.00)	0.19 (0.15)
blank		40.05 (74.60)	59.33 (24.73)	0.47 (0.43)	0.15 (0.24)
AISI 316Ti	N_2	90.83 (77.75)	8.50 (21.78)	0.10 (0.08)	0.56 (0.4)
AISI A213/T91		93.75 (82.06)	5.47 (16.93)	0.00 (0.46)	0.78 (0.55)

nitrate and excessive formation of nitrite and oxide levels. Both corrosion experiments (*316N2Cl* and *213N2Cl*) showed very low nitrite- and high nitrate levels which is opposing the expectations. After opening the crucibles it was observed that molten salt had evaporated in the *blank* experiment and blocked the gas flow into the other crucibles which, in terms of gas connection, were coupled *in-line*. The crucibles containing Solar Salt and AISI A213/T91 / AISI 316Ti (experiments *213N2Cl* and *316N2Cl*) were therefore effectively exposed to the *initial* gas atmosphere and evolving product gases (e.g. during nitrate-nitrite-equilibration) were not removed over the whole course of the experiment. This explains well why the nitrate and nitrite levels rather behave as if stored under (synthetic) air rather than inert atmosphere. Both experiments were repeated with individual gas inlets for each crucible and the expected molten salt degradation was observed in both experiments (see Table 2, experiments *213N2Clr* and *316N2Clr*). Despite failure, all experiments were used for evaluation since the difference in molten salt chemistry can directly be linked to corrosion phenomena observed, as shown later.

In addition to the four anion ions shown in Table 2, the (initially added) chloride levels were also detected by ion chromatography and no measurable loss of chlorides was observed. More importantly however, ion chromatography revealed the presence of an additional anion ions identified as chromate (CrO_4^{2-})-ion. In specific experi-

ments, particularly in *213SACl*, *213SAClr*, *213N2Cl*, and *213N2Clr* but also in experiments containing 316 steel (*316N2*/*316N2r*) significant chromate concentrations were detected.

While the corrosion behavior of martensitic steels in the presence of chloride impurities has been described before by Kleppa and Meschel [26], Dorcheh et al. [27], and for Chilean salts by Fernández et al. [18], the enhanced corrosion of AISI 316Ti in decomposing Solar Salt and the resulting formation of chromates has not been published to our best knowledge. It drastically highlights the impact of molten salt chemistry on the corrosion process and the necessity of monitoring and investigating the molten salt chemistry during and/or after the corrosion experiment.

Corrosion of AISI 316Ti in Solar Salt

To understand the impact of molten salt chemistry on corrosion, images of the samples of AISI 316Ti after exposure to Solar Salt under both atmospheres, with and without chloride impurities were recorded. They are shown in the inlets of Figure 4, the repeated experiments are presented in Figure 11.

When AISI 316Ti is exposed to classical Solar Salt under s.a. (Figure 4, top left) the non-etched (washed) surface appears to be greyish indicating the formation of a homogeneous oxide layer on the surface. Similar results are obtained for both of the experiments using molten salt with chloride impurities (row 3 and 4, left side). However, if AISI 316Ti is exposed to molten salt under a nitrogen atmosphere (Figure 4, row 2, left), spots of red-brownish color appear, which may give rise to the presence of hematite at the surface.[28] The oxide layer appears to be heterogeneous meaning that different oxide scales may be present at the surface.

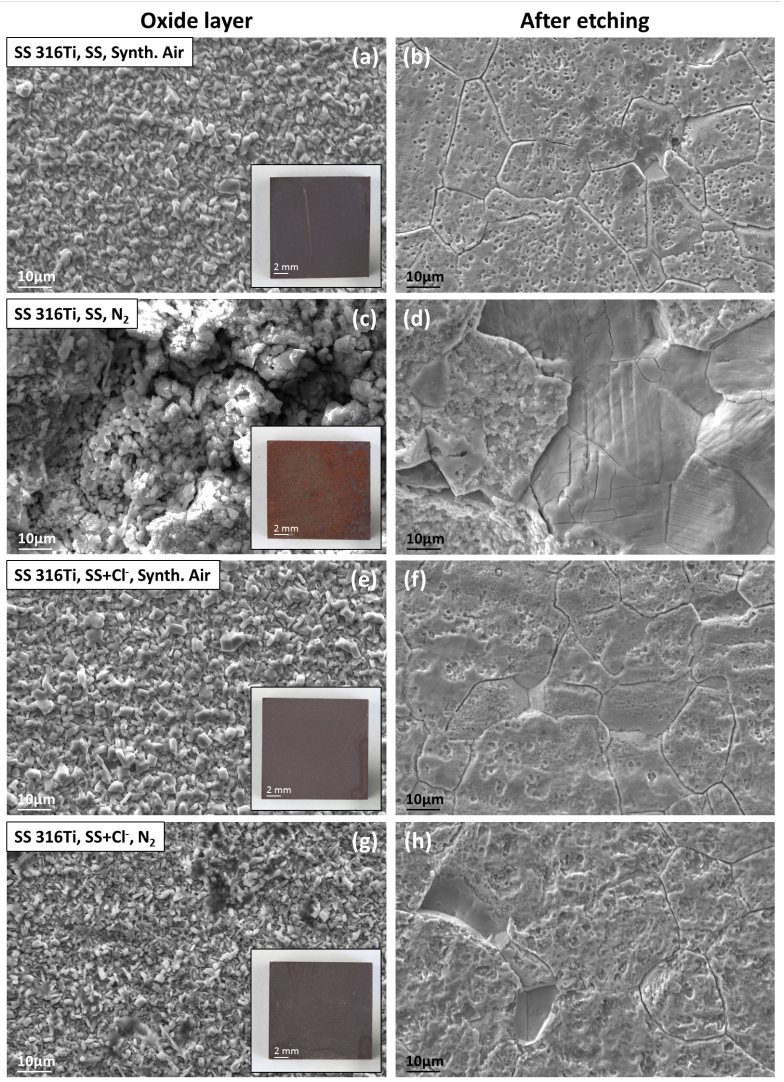

Figure 4: SEM images of AISI 316Ti after the corrosion experiments in Solar Salt (SS) or Solar Salt + chloride impurities (SS+Cl^-) in s.a. or N_2 atmosphere left column: before etching including the oxide layer and right column: after etching. Inlets show images of the extracted and washed steel samples.

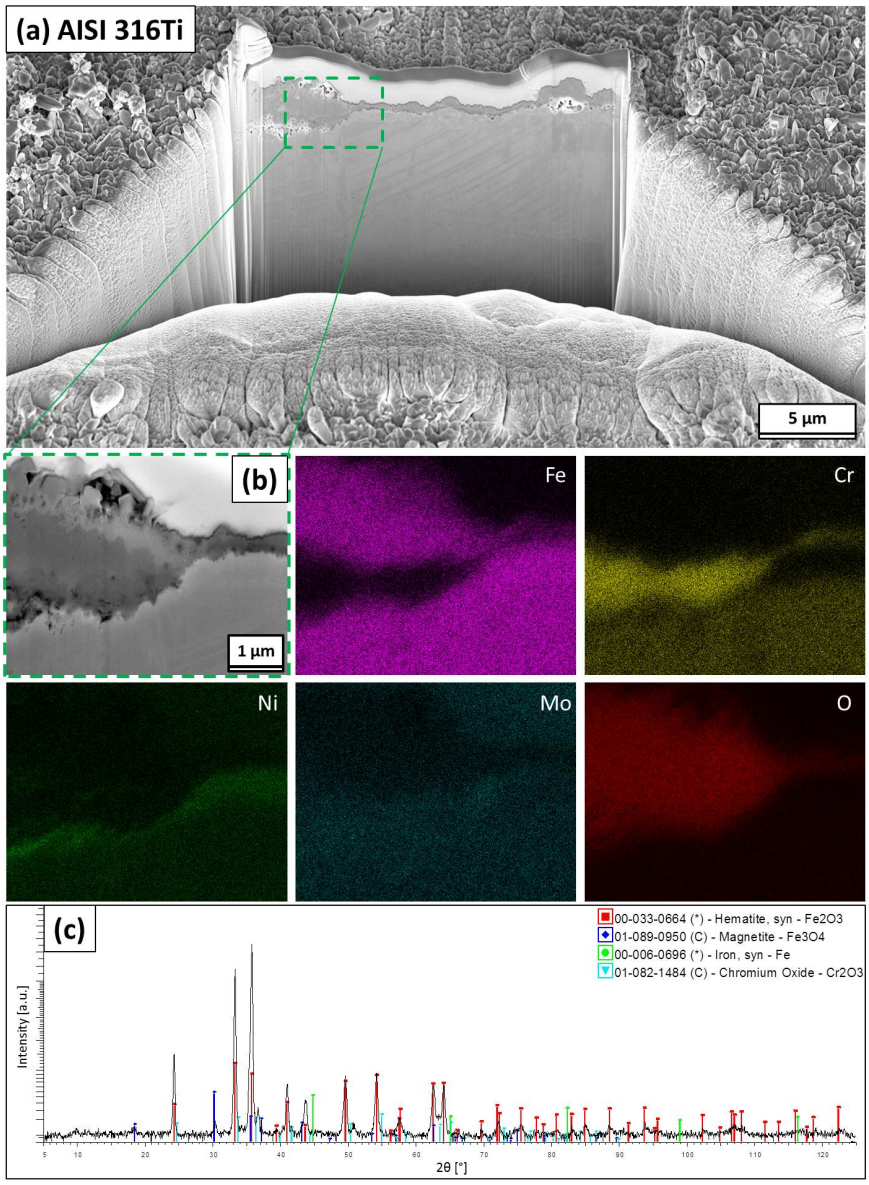

Figure 5: (a) SEM image of a FIB-cut AISI 316Ti sample exposed to Solar Salt at 560 °C under synthetic air for 1008 h. (b) BSE image of a zoom into the sample as well as EDX mappings for different elements (as labelled) in the same area. (c) XRD pattern of the same sample after the corrosion experiment.

The structure of the oxide scales is known from experiments performed previous to the ones presented here, where conditions were identical with slightly shorter exposure

times of 1008 h. An SEM image of AISI 316Ti cut with focused ion beam (FIB) to produce a polished cross section, is shown in Figure 5(a). The sample exhibits a similar surface structure compared to the sample of experiment *316SA*, indicating the difference in exposure time is negligible. From the cross-section clear signs of breakaway oxidation (see e.g. ref. [29]) are indicated by the strongly varying thickness of the oxide scale. A zoom into the cross section and EDX-analysis of the respective area are shown in Figure 5(b). The outer oxide layer consists of iron oxides with an inner layer of chromium oxide. At the sub-scale interface Cr depletion and Ni-enrichment is evident from the Cr and Ni maps.

XRD pattern of the AISI 316Ti sample (Figure 5) show the formation of hematite (Fe_2O_3) and magnetite (Fe_3O_4) and presumably Cr_2O_3. Displacement of the reflections from ideal positions may be indicative of the presence of mixed iron-chromium oxides. Overall, the SEM-EDS and XRD results display typical oxide layer formation with multi-layered structures containing an outer Cr-free magnetite- or hematite-layer as well as an inner Fe-Cr-spinel ($FeCr_2O_4$-type) or even pure Cr_2O_3 layer.[20, 30, 31]

For the AISI 316Ti sample stored under nitrogen atmospheres (*316N2*) the observed change in surface structure and corrosion rate may give rise to a different corrosion mechanism. In fact, the corrosion rate (Table 3) increases by a factor of 5 as compared to experiments under s.a. (*316SA*). Additionally, the surface shows signs of local corrosion attack reflected by heterogeneous surface structures (Figure 4, row 2, right) visible after etching. The other three samples (Figure 4(b), (f), (h)) show typical signs of sensitization with pronounced grain boundaries and beginning intergranular attack.

The changing corrosion mechanism upon the switch from s.a. to N_2 atmospheres can be ascribed to a significant change of the molten salt chemistry. As explained earlier, the content of nitrites and oxides in the molten salt is much higher under N_2 than under air. This is supported by the fact that an increasing level of chromates is detected in the molten salt samples for the experiments under N_2 (*316N2* and *316N2r*), while no chromates (CrO_4^{2-}) are detected in any other experiment containing SS 316Ti. This behavior is not intuitive but can be explained by the special chemistry of chromium in molten nitrate and nitrite salts. Brough and Kerridge [32], Brough et al. [33], Eweka

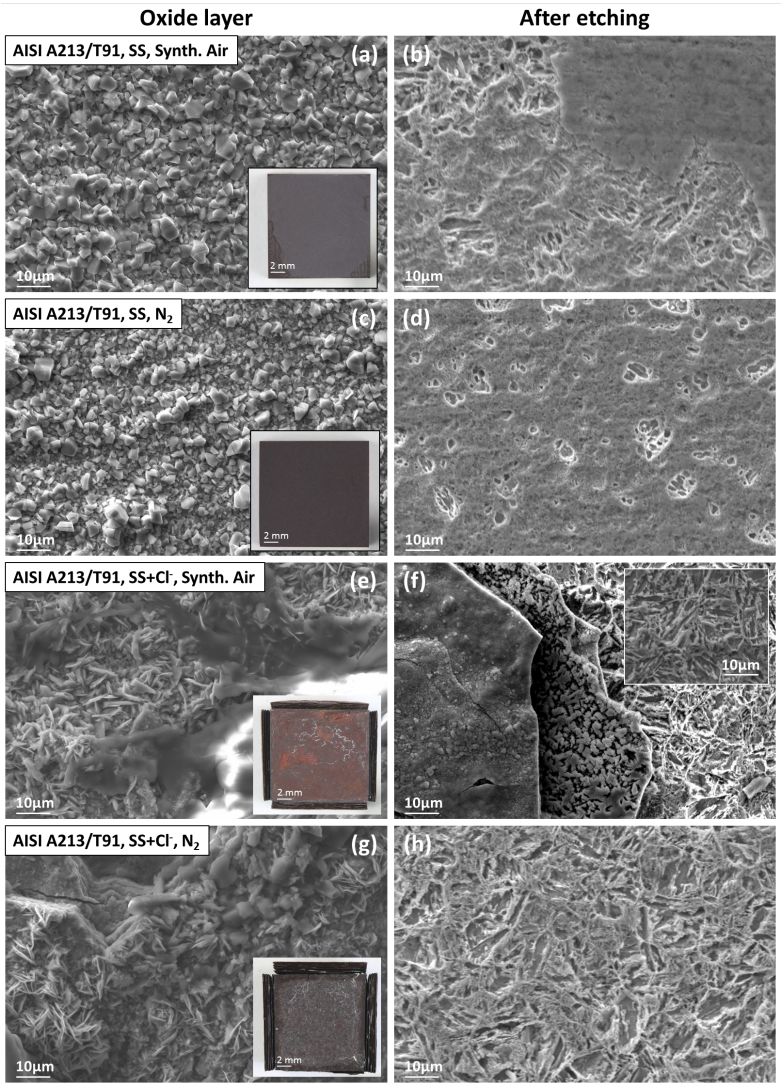

Figure 6: SEM images of AISI A213/T91 after the corrosion experiments in Solar Salt (SS) or Solar Salt + chloride impurities (SS+Cl^-) in s.a. or N_2 atmosphere left column: before etching including the oxide layer and right column: after etching. Inlets show images of the extracted and washed steel samples.

Table 3: Corrosion rates, chromate content, nitrite formation rate and final nitrite content in Solar Salt.

Exp.-ID	Gas	Corrosion rate [$\mu m\,a^{-1}$]	CrO_4^{2-} content [wt %]	$d[NO_2^-]/dt$ [mol % h^{-1}]	NO_2^- content‡ [mol %]
blankSA	s.a.	-	-	0	4.37
316SA		18.81	-	0	5.31
316SAr		10.55	-	0	4.74
213SA		16.91	-	0	5.20
213SAr		21.91	-	0	5.02
blankN2	N_2	-	-	0.037	35.97
316N2		104.63	0.067	0.050*	49.90
316N2r		91.24	<0.03	0.048*	50.35
213N2		14.59	-	0.024	27.91
213N2r		76.72	-	0.036†	42.61
blankSACl	s.a.	-	-	0	4.92
blankSAClr		-	-	0	5.66
316SACl		22.86	-	0	5.24
316SAClr		15.21	-	0	6.28
213SACl		1377.56	0.215	0	4.31
213SAClr		2495.91	0.358	0	4.74
blankN2Cl	N_2	-	-	0.048#	59.33
blankN2Clr		-	-	0.020#	24.73
316N2Cl		18.42	-	0.006	8.51
316N2Clr		32.54	-	0.017	21.78
213N2Cl		1865.16	0.248	0.004	5.47
213N2Clr		2398.08	0.380	0.013	16.93

‡: NO_2^- content at the end of the experiment

∗: between 0 h to 800 h

†: non-linear behavior

#: extrapolated assuming a starting content of 1.2 mol % and a linearly increasing nitrite content

and Kerridge [34, 35] reported extensively that the main reactions of chromium in nitrate/nitrite salts are the following:

1. pure Cr_2O_3 reacts with nitrate ions to form chromate (CrO_4^{2-}) without intermediate dichromate ($Cr_2O_7^{2-}$) formation
2. pure Cr^0 reacts in nitrate melts to form dichromate at temperatures below 400 °C
   - during this reaction *no* intermediate Cr_2O_3 is formed [33]
   - dichromate *preferentially* reacts with nitrite to form chromate [33, 36]

These results contradict the commonly accepted corrosion mechanism where the nitrate ion is assumed to convert iron and chromium to the respective oxides. From our

work and the presented literature review we suggest a different corrosion mechanism: during the first interaction of molten nitrate salt with exposed bulk material (after local spalling of the oxide scale) the classical iron oxidation occurs, as mentioned in Eq. 3. Available chromium can react to form dichromates according to the following equation:

$$2Cr^0 + 7NO_3^- \longleftrightarrow Cr_2O_7^{2-} + 5NO_2^- + 2NO_2 \tag{7}$$

The follow-up reaction to form chromates according to Eq. 8

$$Cr_2O_7^{2-} + 2NO_2^- \longleftrightarrow 2CrO_4^{2-} + NO_2 + NO \tag{8}$$

as described by Brough et al. [33] occurs subsequently and is limited by the presence of nitrite ions and as demonstrated in this work, the nitrite concentration is substantially higher under N_2 compared to s.a.. It therefore appears that the rate limiting step in the reaction of chromium metal to chromates is the intermediate conversion of dichromates with nitrites to form chromates (Eq. 8). Under s.a. the nitrite ions are much more diluted in the nitrate melt than under N_2, which leads to slower reaction kinetics and thus lower, or even no, formation of chromates. The second important statement of Brough's work however is that chromium oxide is not directly formed by the oxidation of Cr^0 with nitrate, so the origin of Cr_2O_3-formation in the first place has to be assessed. From the electrochemical potentials of iron and chromium we would rather propose that chromium oxide is formed by the redox reaction:

$$Cr^0 + 3Fe^{3+} \longleftrightarrow Cr^{3+} + 3Fe^{2+} \tag{9}$$

with the reaction exhibiting an electrochemical potential of 1.53 V at room temperature. The redox potentials, although not to be taken for granted due to the higher temperature and different electrolyte, indicate that Fe^{III} can oxidize Cr^0 to form Fe^{II} and Cr^{III}. Since direct Cr_2O_3 formation from oxidation by nitrate seems unlikely, this mechanism may be a feasible reaction path, which has not been discussed in literature to our best knowledge. It would be supported by studies which shows that chromium diffusion into the oxide layers and eventually chromia-formation occurs at the interface between oxide scales and bulk material, measurably after iron oxides were formed.[30]

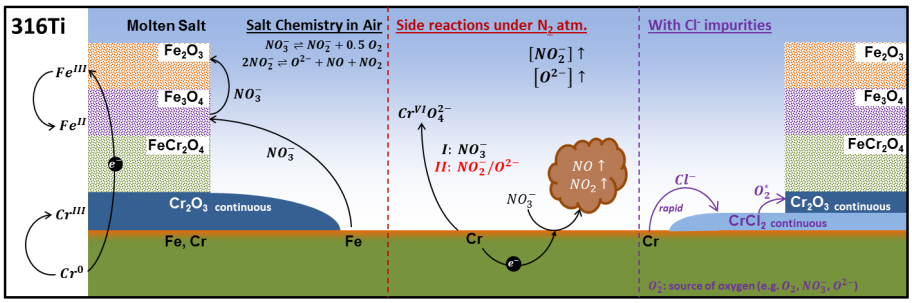

Figure 7: Proposed corrosion mechanism of AISI SS316Ti in Solar Salt at 560 °C under synthetic air- (left), under N_2-atmosphere (middle), and in Solar Salt containing chloride impurities for both atmospheres, s.a. and N_2 (right).

The proposed corrosion mechanisms of SS316Ti in air and N_2 atmosphere described are schematically shown in Figure 7.

Overall, the corrosion rates of 316Ti in molten salt under air atmospheres are relatively low ($< 15\,\mu m\,a^{-1}$ to $20\,\mu m\,a^{-1}$) both with (*316SACl*) and without (*316SA*) chloride impurities present in the molten salt. Under nitrogen atmospheres chloride impurities seem to induce a protective character, as reflected by a significantly lower corrosion rate ($CR_{316N2Cl} < CR_{316N2}$ and $CR_{316N2Clr} < CR_{316N2r}$). This may result from a faster mass transport due to the formation of chromium chlorides ($CrCl_2$) leading to a faster (re-)formation of a protective Cr_2O_3-layer, proposed by Dorcheh et al. [27].

In the case of Solar Salt with chlorides under N_2 (Figure 4, bottom left) however the repeated experiment (*316N2Clr*) showed different results in that the surface shows signs of pitting corrosion and heterogeneous surface structures. This is well in line with the corrosion rates of the different samples. Therein, the sample under nitrogen without chloride impurities (*316N2r*) showed far higher corrosion rates than the other three stainless steel samples (*316SAr*, *316SAClr*, and *316N2Clr*). Together with the formation of chromates, this result is of high relevance for molten salt utilization in the CSP sector since it reflects that the salt chemistry has a tremendous influence on the corrosion resistance of AISI 316Ti.

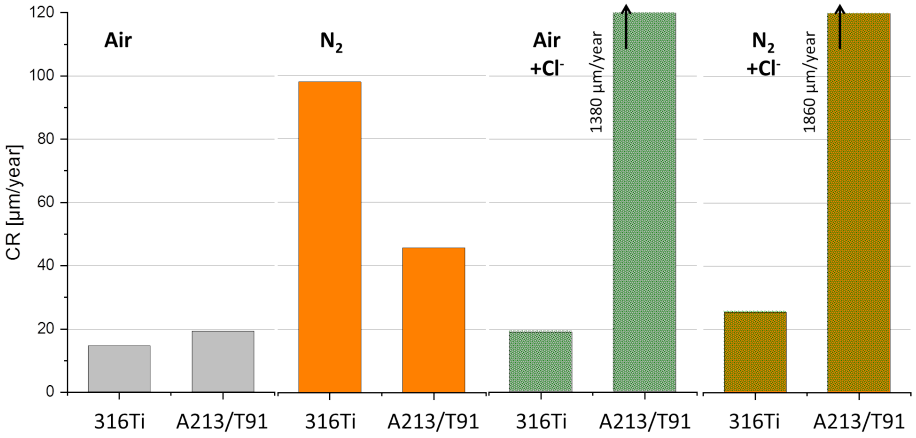

Figure 8: Average corrosion rates of AISI A213 and AISI 316Ti from original and repeated experiments.

Corrosion of AISI A213/T91 in Solar Salt

Regarding the surfaces of A213/T91 after exposure to molten salt under s.a. and N_2 atmosphere, a homogeneous grey oxide layer has formed (Figure 6), which is assumed to be hematite. If chloride impurities are present in the molten salt (*213SAClr* & *213N2Clr*), thicker and non-adherent oxide layers are formed indicating that no protective layer is formed and further oxidation is promoted. The color changes from greyish without chlorides, to brownish when chlorides are present, but it has to be emphasized that the color of most Fe oxides is highly sensitive to crystal impurities and defects.[37]

The SEM-EDX analysis and XRD pattern of AISI A213/T91 exposed to Solar Salt at 560 °C under synthetic air for 1008 h is shown in Figure 9. As in the case of 316Ti, the thickness of the oxide layer is non-uniform with signs of breakaway oxidation. Fe and Cr maps shown Fe enrichment towards the outer oxide layer and Cr enrichment towards the inner part of the oxide layer. The maps may indicate a mixed Fe,Cr-oxide most likely a $FeCr_2O_4$-spinel. All of which is supported by XRD analysis (Figure 9(c)) which shows the presence of hematite (Fe_2O_3) and magnetite (Fe_3O_4). The broadness of the reflections may however indicate a mixed crystal structure that is distorted by the presence of chromium, which is in agreement with the Cr and Fe distribution maps. It is commonly accepted, that martensitic high temperature steel A213/T91 forms a

spinel containing Fe- and Cr-oxide, since its chromium content of max. 9.5 % is too low to form a pure Cr-oxide layer [21].

This spinel exhibits a less protective character than the pure Cr-oxide layer on the stainless steel surface and further oxidation might occur.[21] In fact, our results show a generally higher corrosion rate of A213/T91 as compared to 316Ti. Under the presence of chlorides, this difference is especially pronounced and the corrosion rates increase from $20/40\,\mu m\,a^{-1}$ (under air/N_2 without chlorides) to $>1380\,\mu m\,a^{-1}$. The mechanism is similar to that described for SS316 with the only difference being the low overall concentration of Cr in A213/T91. The latter leads to the formation of a non-continuous and non-protective Cr_2O_3 layer, as described by Dorcheh et al. [27] in more detail, that most likely is oxidized to CrO_4^{2-} immediately. The different corrosion mechanisms are shown in Figure 10.

The molten salt analysis displayed typical nitrate-nitrite levels for all samples under s.a., but additionally a significant amount of chromate ions is detected in molten salts containing chloride impurities after contact with A213/T91 (*213SACl*, *213SAClr*, *213N2Cl*, and *213N2Clr*). The chromate concentrations are in a range above 0.2 wt % (Table 3) indicating severe depletion of chromium from the steel sample into the molten salt. Given the known geometry and density of the steel sample and the molten salt mass, it could be estimated that 11 % of the total chromium content of the steel sample formed soluble chromates (>19 % in the repeated experiments).

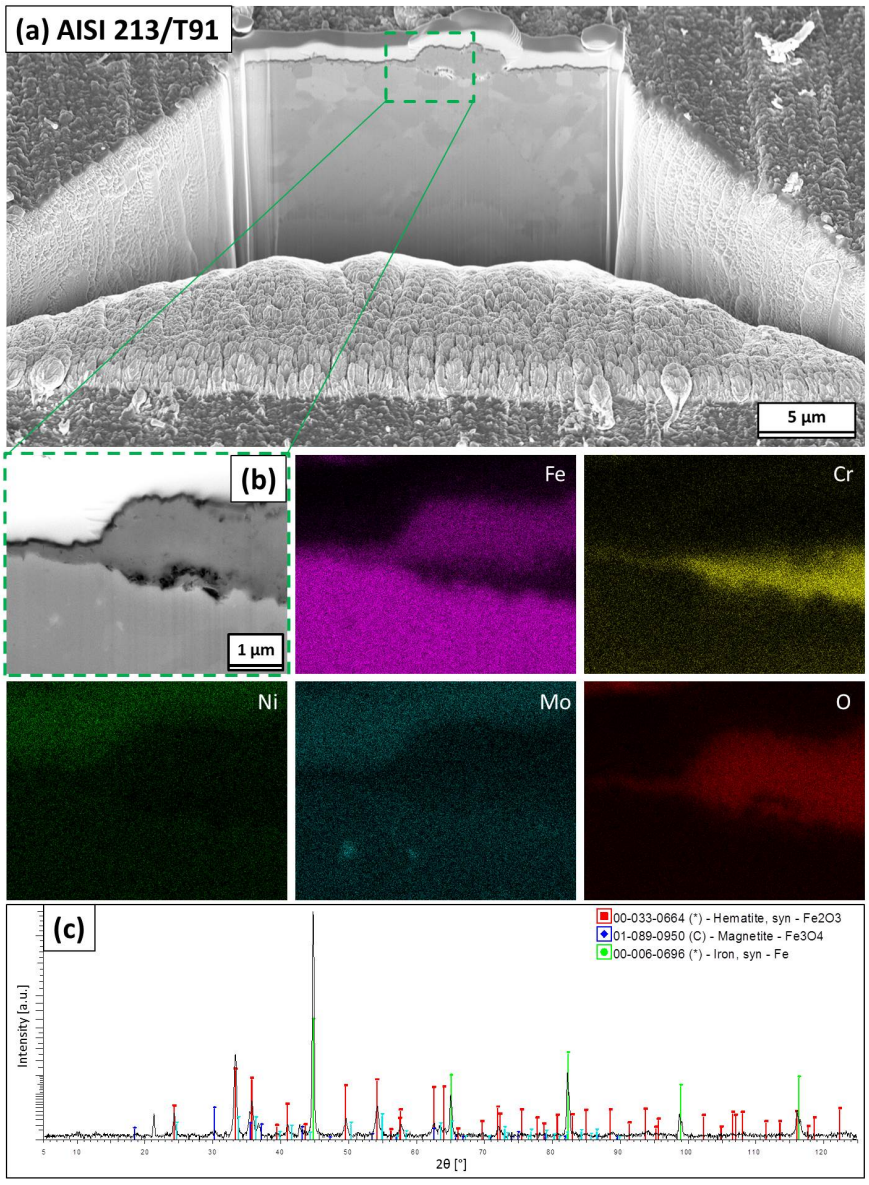

Figure 9: (a) SEM image of a FIB-cut AISI A213/T91 sample exposed to Solar Salt at 560 °C under synthetic air for 1008 h from a different, unpublished study by the authors of this manuscript. (b) BSE image of a zoom into the sample as well as EDX mappings for different elements (as labelled) in the same area. (c) XRD pattern of the same sample after the corrosion experiment.

Hereafter we attempt to explain the corrosion mechanism based on existing litera-

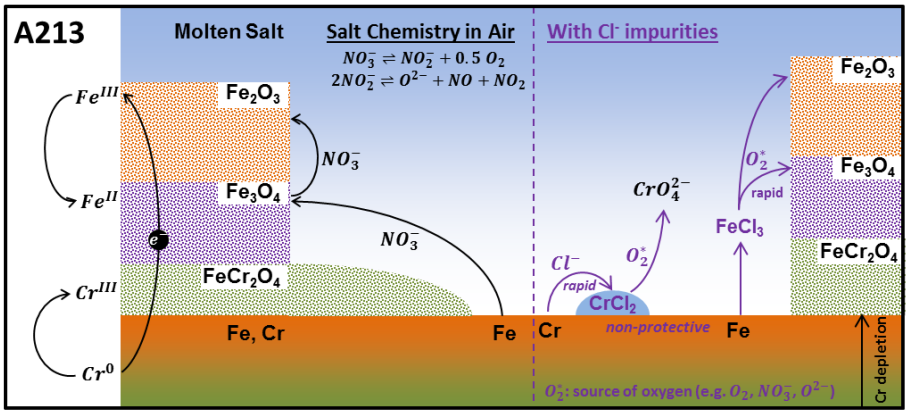

Figure 10: Proposed corrosion mechanism of AISI A213/T91 in Solar Salt at 560 °C under synthetic air- (left) and in Solar Salt containing chloride impurities for both atmospheres, s.a. and N_2 (right).

ture and the results gained in this work. As mentioned, chlorides enhance mass transport thereby increasing the oxide formation kinetics.[38] More precisely iron chlorides ($FeCl_x$) exhibit a higher vapour pressure than chromium chlorides ($CrCl_x$) and, according to Liu, require "a significantly higher oxygen pressure to convert to iron oxide" [38]. These chlorides are typically formed at the interface of molten salt with the bulk material, which in the case of A213/T91 is covered by a non-protective spinel layer. Consequently, iron chlorides can diffuse outward and iron oxides are (re-)formed further away from the bulk material leading to the formation of porous oxide layers, which increases the unprotected surface area. Chromium from the bulk material can also react to form chlorides but may as well be oxidized to chromates e.g. as proposed by Brough et al. [33] by the reaction with nitrate ions (Eq. 10). Interestingly in Brough's work it is stated, that an intermediate reaction of chromium metal to form Cr_2O_3 can be excluded, which may as well be the case for the work here. In contrast to Brough's work, we do not expect the intermediate formation of $Cr_2O_7^{2-}$, since it is not stable at temperatures above 400 °C and immediately oxidizes to form chromates (CrO_4^{2-})[36] which, again, is limited by the presence of nitrite ions.

$$Cr^0 + 7NO_3^- \rightleftharpoons CrO_4^{2-} + 3NO_2^- + NO_2 + NO \tag{10}$$

Overall it can therefore be stated that the atmosphere alone (in the absence of chlorides) has an impact on the corrosion of A213/T91, with higher corrosion rates under N_2 ($CR_{213N2r} = 77\,\mu m\,a^{-1}$) than in s.a. ($CR_{213SAr} = 20\,\mu m\,a^{-1}$). In both experiments Cr dissolution is not relevant (at least up to 1200 h under given conditions). The addition of chloride impurities leads to catastrophic deterioration and extreme depletion of chromium (e.g. *213SACl*, *213N2Cl*), forming soluble chromates in the molten salt. Yet, there is no agreement on the exact corrosion mechanism but we support the statement that chloride impurities enhance mass transport[38] and that formation of a protective Cr_2O_3 scale is hindered by the overall low concentration of chromium in the bulk metal.

4. Conclusions

This study investigated the influence of molten salt chemistry and the impurity "chloride" on the corrosion behavior of martensitic A213/T91 and austenitic SS 316Ti. The molten salt chemistry could directly be affected by the composition of the overflowing atmosphere. In this study a synthetic air atmosphere was compared to N_2 atmosphere. In the first case a stable nitrate/nitrite level was obtained while in the latter case, excessive nitrate decomposition, nitrite formation and oxide formation occur. The salt composition was monitored throughout the corrosion studies and later linked to the corrosion phenomena observed. As one of the first authors we have demonstrated that the molten salt aging has a direct impact on not only the corrosion rate, but also on the corrosion mechanism. In contrast to earlier studies, chromium dissolution was observed during the corrosion of SS 316Ti in Solar Salt stored under N_2 atmosphere, which was ascribed to unusually high nitrite and oxide contents, formed by the steady decomposition of the nitrate melt. Eventually, it may be necessary to reassess the role of chromium in the corrosion process and therefore the corrosion mechanism itself.

A213/T91 showed a higher sensitivity to the presence of chloride impurities which is reflected by excessive chromium dissolution and corrosion rates significantly above $1\,mm\,a^{-1}$ ($< 30\,\mu m$ without chloride impurities). It could be estimated that at least 11 % of the total chromium content of the steel sample leaked into the molten salt to

form chromates. Chloride impurities can therefore have a tremendous impact on the lifetime of the CSP plant, but further studies are required to elucidate this hypothesis. Overall, the results obtained demonstrated that it is essential to monitor the molten salt chemistry and the corrosion attack simultaneously. Only then the impact of attacking medium including impurities onto the corrosion mechanism and the dissolution of alloying elements can be studied entirely and in relation to one another.

Acknowledgment

The authors thank the German Federal Ministry for Economic Affairs and Energy for the financial support given to this work in the MS-STORE project (Contract No. 0325497 A/B). The research leading to these results has received funding from the European Union Seventh Framework Program FP7/2007-2013 under grant agreement no. 609837. Technical assistance from Ulrike Kröner (DLR Stuttgart) is greatly appreciated. We kindly thank Sabine Sturm at MPA University of Stuttgart for metallographic preparation and Jochen Forstner for extensive molten salt analysis.

References

[1] S. Kuravi, J. Trahan, D. Y. Goswami, M. M. Rahman, E. K. Stefanakos, Thermal energy storage technologies and systems for concentrating solar power plants, Progress in Energy and Combustion Science 39 (2013) 285–319. doi:10.1016/j.pecs.2013.02.001.

[2] Y. Tian, C. Zhao, A review of solar collectors and thermal energy storage in solar thermal applications, Applied Energy 104 (2013) 538–553. URL: http://www.sciencedirect.com/science/article/pii/S0306261912008549. doi:10.1016/j.apenergy.2012.11.051.

[3] V. S. Reddy, S. Kaushik, K. Ranjan, S. Tyagi, State-of-the-art of solar thermal power plants - a review, Renewable and Sustainable Energy Reviews 27 (2013) 258 – 273. doi:https://doi.org/10.1016/j.rser.2013.06.037.

[4] A. Bonk, S. Sau, N. Uranga, M. Herainz, T. Bauer, Advanced heat transfer fluids for direct molten salt line-focusing csp plants, Progress in Energy and Combustion Science 67C (2018) 69–87.

[5] K. Vignarooban, X. Xu, A. Arvay, K. Hsu, A. Kannan, Heat transfer fluids for concentrating solar power systems ï£¡ a review, Applied Energy 146 (2015) 383 – 396. URL: http://www.sciencedirect.com/science/article/pii/S0306261915001634. doi:https://doi.org/10.1016/j.apenergy.2015.01.125.

[6] T. Bauer, P. Nicole, D. Laing, High temperature molten salts for solar power application, in: Molten Salts Chemistry, Elsevier, 2013, pp. 415–439. doi:10.1016/B978-0-12-398538-5.00020-2.

[7] T. Bauer, N. Pfleger, N. Breidenbach, M. Eck, D. Laing, S. Kaesche, Material aspects of solar salt for sensible heat storage, Applied Energy 111 (2013) 1114–1119. URL: http://linkinghub.elsevier.com/retrieve/pii/S0306261913003681.

[8] D. Nissen, D. Meeker, Nitrate-nitrite chemistry in $NaNO_3$-KNO_3 melts, Inorganic Chemistry 22 (1983) 716–721.

[9] A. Bonk, C. Martin, M. Braun, T. Bauer, Material investigations on the thermal stability of solar salt and potential filler materials for molten salt storage, AIP Conference Proceedings 1850 (2017) 080008: 1–8. doi:10.1063/1.4984429, aIP conference proceedings.

[10] R. Bradshaw, D. Dawson, W. De la Rosa, R. Gilbert, S. e. a. Goods, SAND2002-0120: Final Test and Evaluation Results from the Solar Two Project, resreport, Sandia National Laboratories, 2002.

[11] E. S. Freeman, The kinetics of the thermal decomposition of potassium nitrate and of the reaction between potassium nitrite and oxygen 1a, Journal of the American Chemical Society 79 (1957) 838–842. URL: http://pubs.acs.org/doi/abs/10.1021/ja01561a015.

[12] K. H. Stern, High temperature properties and decomposition of inorganic salts - part 3 nitrates and nitrites, Journal of Physical and Chemical Reference Data 1 (1972) 748–772.

[13] C. Yang, X. Wei, W. Wang, Z. Lin, J. Ding, Y. Wang, Q. Peng, J. Yang, Nox emissions and the component changes of ternary molten nitrate salts in thermal energy storage process, Applied Energy 184 (2016) 346–352.

[14] A. Baraka, A. I. Abdel-Rohman, A. A. El Hosary, Corrosion of mild steel in molten sodium nitrate-potassium nitrate eutectic, British Corrosion Journal 11 (1975) 44–46.

[15] J. M. De Jong, G. H. J. Broers, A reversible oxygen electrode in an equimolar KNO_3-$NaNO_3$ melt saturated with sodium peroxide - ii. a voltammetric study, Electrochimica Acta 21 (1976) 893–900. doi:10.1016/0013-4686(76)85062-1.

[16] E. Desimoni, F. Paniccia, P. Zambonin, Solubility and detection (down to 30 p.p.b.) of oxygen in molten alkali nitrates, Journal of Electroanalytical Chemistry and Interfacial Electrochemistry 38 (1972) 373–379. URL: http://linkinghub.elsevier.com/retrieve/pii/S0022072872803474.

[17] E. Desimoni, F. Paniccia, L. Sabbatini, P. G. Zambonin, Hydrogen half-cells in molten salts. a potentiometric investigation of the systems Pt or Au) H_2O/H_2, OH^- in fused alkali nitrates, Journal of Applied Electrochemistry 6 (1976) 445–451. URL: http://link.springer.com/10.1007/BF00616544.

[18] A. Fernández, H. Galleguillos, F. Pérez, Thermal influence in corrosion properties of chilean solar nitrates, Solar Energy 109 (2014) 125 – 134. URL: http://www.sciencedirect.com/science/article/pii/S0038092X14003764. doi:https://doi.org/10.1016/j.solener.2014.07.027.

[19] L. Singheiser, Hochtemperaturkorrosion durch Salzschmelzen, WILEY-VCH Verlag GmbH & Co. KGaA, 2001, pp. 542–572. doi:10.1002/9783527625659.fmatter.

[20] A. G. Fernández, M. I. Lasanta, F. J. Pérez, Molten salt corrosion of stainless steels and low-cr steel in csp plants, Oxidation of Metals 78 (2012) 329–348. URL: https://doi.org/10.1007/s11085-012-9310-x. doi:10.1007/s11085-012-9310-x.

[21] L. Pinder, K. Dawson, G. Tatlock, High Temperature Corrosion of Low Alloy Steels, Elsevier, 2010, pp. 558–582. doi:https://doi.org/10.1016/B978-044452787-5.00075-5.

[22] A. Bonk, M. Braun, A. Hanke, J. Forstner, D. Rückle, S. Kaesche, V. Sötz, T. Bauer, Influence of different atmospheres on molten salt chemistry and its effect on steel corrosion, AIP conference proceedings (2018). doi:https://doi.org/10.1063/1.5067097.

[23] DIN 50905-1:2009-09 Corrosion of metals - Corrosion testing - Part 1: General guidance, 2009.

[24] Á. G. Fernández, L. F. Cabeza, Molten salt corrosion mechanisms of nitrate based thermal energy storage materials for concentrated solar power plants: A review, Solar Energy Materials and Solar Cells 194 (2019) 160–165. doi:10.1016/j.solmat.2019.02.012.

[25] Y. Dessureault, J. Sangster, A. D. Pelton, Coupled phase diagram-thermodynamic analysis of the 24 binary systems, a2co3-AX and a2so4-AX where a=li, na, k and x=cl, f, NO3, OH, Journal of Physical and Chemical Reference Data 19 (1990) 1149–1178. doi:https://doi.org/10.1063/1.555866.

[26] O. J. Kleppa, S. V. Meschel, Thermochemistry of anion mixtures in simple fused salt systems. ii. solutions of some salts of MO_4^- and MO_4^{2-} anions in the corresponding alkali nitrates, The Journal of Physical Chemistry 67 (1963) 2750–2753.

URL: https://doi.org/10.1021/j100806a057. doi:10.1021/j100806a057. arXiv:https://doi.org/10.1021/j100806a057.

[27] A. S. Dorcheh, R. N. Durham, M. C. Galetz, High temperature corrosion in molten solar salt: The role of chloride impurities, Materials and Corrosion 68 (2017) 943–951. URL: http://dx.doi.org/10.1002/maco.201609300.

[28] S. Goods, R. Bradshaw, Corrosion of stainless steels and carbon steel by molten mixtures of commercial nitrate salts, Journal of Materials Engineering and Performance 13 (2004) 78–87.

[29] H. E. Evans, A. T. Donaldson, T. C. Gilmour, Mechanisms of breakaway oxidation and application to a chromia-forming steel, Oxidation of Metals 52 (1999) 379–402. URL: https://doi.org/10.1023/A:1018855914737. doi:10.1023/A:1018855914737.

[30] A. Galerie, High Temperature Corrosion of Chromia-forming Iron, Nickel and Cobalt-base Alloys, Elsevier, 2010, pp. 583–605. doi:https://doi.org/10.1016/B978-044452787-5.00076-7.

[31] P. Hou, Oxidation of Metals and Alloys, Elsevier, 2010, pp. 195–239. doi:https://doi.org/10.1016/B978-044452787-5.00013-5.

[32] B. J. Brough, D. H. Kerridge, Reactions of metals in fused nitrate eutectic, Inorganic Chemistry 4 (1965) 1353–1356. doi:10.1021/ic50031a026.

[33] B. Brough, D. Kerridge, S. Tariq, Molten lithium-potassium nitrate eutectic: the reactions of some compounds of chromium, Inorganica Chimica Acta 1 (1967) 267–270.

[34] E. Eweka, D. Kerridge, Molten lithium nitrate-potassium nitrate eutectic: The reaction of chromium(iii) chloride and nickel(ii) chloride, Thermochimica Acta 246 (1994) 117 – 121. URL: http://www.sciencedirect.com/science/article/pii/0040603194850976. doi:https://doi.org/10.1016/0040-6031(94)85097-6.

[35] E. Eweka, D. Kerridge, Molten sodium nitrite-sodium nitrate-potassium nitrate eutectic: the reactions and spectra of chromium(III) chloride and chromium(VI) compounds, Thermochimica Acta 262 (1995) 95–100. doi:10.1016/0040-6031(95)02288-d.

[36] D. Kerridge, S. Tariq, Molten sodium nitrite-potassium nitrite eutectic: the reactions of some compounds of chromium, Inorganica Chimica Acta 3 (1969) 667–670. doi:https://doi.org/10.1016/S0020-1693(00)92574-X.

[37] S. P. Tandon, J. P. Gupta, Diffuse reflectance spectrum of ferric oxide, Spectroscopy Letters 3 (1970) 297–301. doi:10.1080/00387017008078624.

[38] Y. Liu, W. Fan, X. Zhang, X. Wu, High-temperature corrosion properties of boiler steels under a simulated high-chlorine coal-firing atmosphere, Energy & Fuels 31 (2017) 4391–4399. doi:https://doi.org/10.1021/acs.energyfuels.6b02755.

5. Supplementary Material

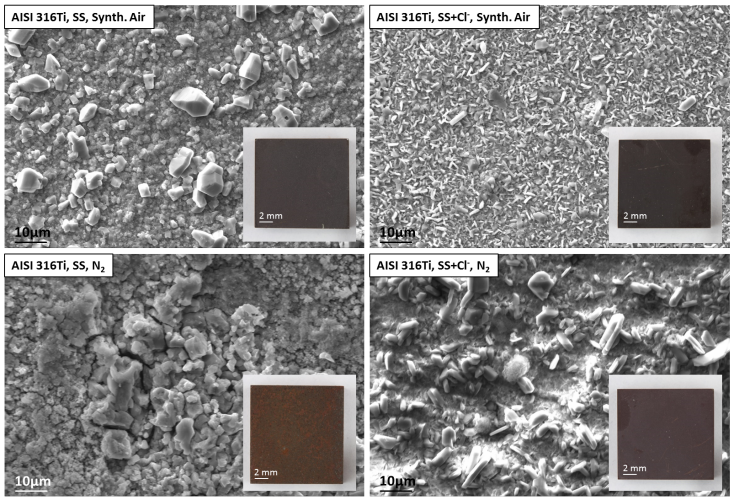

Figure 11: SEM images of non-etched AISI 316Ti from repeated experiments following the same methodology as the one presented in Figure 4.

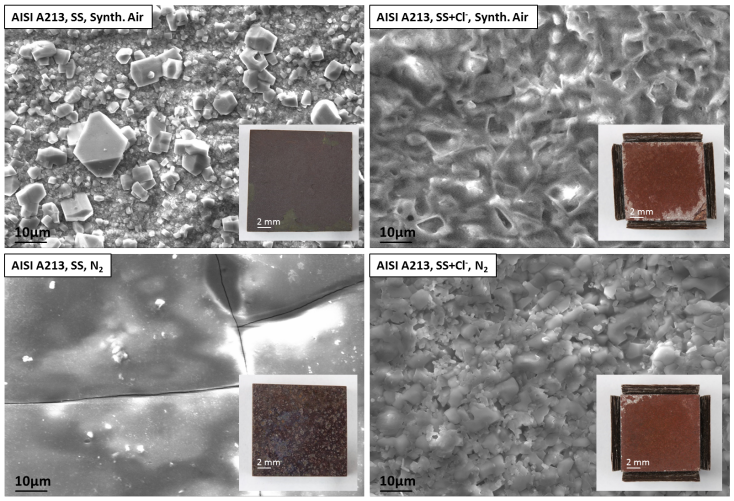

Figure 12: SEM images of non-etched A213/T91 from repeated experiments following the same methodology as the one presented in Figure 4.